RESEARCH ARTICLE | MAY 08 2023

Spectral current density and responsivity scaling for Fourier transform photocurrent spectroscopy

J. Kunc ✉ 🔾 ; B. Morzhuk 🔾 ; M. Shestopalov 🔾 ; T. Fridrišek 🔾 ; V. Dědič 🔾

Check for updates

View Online   Export Citation   CrossMark

Spectral current density and responsivity scaling for Fourier transform photocurrent spectroscopy

View Online   Export Citation   CrossMark

J. Kunc,[a] ⓘ B. Morzhuk, ⓘ M. Shestopalov, ⓘ T. Fridrišek, ⓘ and V. Dědič ⓘ

AFFILIATIONS

Faculty of Mathematics and Physics, Institute of Physics, Charles University, Ke Karlovu 5, CZ-121 16 Prague 2, Czech Republic

[a]Author to whom correspondence should be addressed: kunc@karlov.mff.cuni.cz

ABSTRACT

We propose and experimentally verify a methodology to scale arbitrary units to photocurrent spectral density (A/eV) in Fourier transform Photocurrent (FTPC) spectroscopy. We also propose the FTPC scaling to responsivity (A/W), provided a narrow-band optical power measurement is available. The methodology is based on an interferogram waveform consisting of a constant background and interference contribution. We also formulate conditions that have to be met for correct scaling. We experimentally demonstrate the technique on a calibrated InGaAs diode and weak responsivity, long response time SiC interdigital detector. We identify a series of impurity-band and interband transitions in the SiC detector and slow mid-gap to conduction band transitions.

25 January 2024 11:45:21

I. INTRODUCTION

Fourier transform Photocurrent (FTPC) spectroscopy is a sensitive experimental technique to study semiconductors,[1–3] hydrogen-related shallow impurities,[4,5] micro-crystalline silicon for solar cells,[3] quantum dots,[6,7] nano-diamond thin layers,[8] or emerging materials, such as perovskites.[9,10] The FTPC is closely related to Photo-thermal Ionization Spectroscopy (PTIS), which aims to study impurities in high-purity semiconductors,[1,11] including their local field interactions by applying magnetic fields.[2] Later, the technique started to be used to measure spectral-resolved photoconductivity[3,12,13] with the advantages of higher spectral resolution, higher sensitivity, and faster measurement compared to monochromator-based techniques. However, despite their advantages, the FTPC and PTIS lack a photocurrent and responsivity scaling method.

There were attempts to scale the spectral current density of solar cells.[13] However, here, the authors measured a short-circuit current of the solar cell. That is inapplicable to samples with weak responsivity, frequency, or spectrally dependent response time. Other attempts matched the high-energy spectrum with the transmittance and reflectance data, scaling the FTPC to the absorption units (cm^{-1}) or matching the FTPC and monochromator-based photoconductivity.[14]

However, these scaling techniques require high photocurrents or supplementary experiments. The additional experiments diminish the advantages of FTPC spectroscopy, such as fast acquisition times and high dynamical range. These issues typically lead to arbitrary unit scaling of the FTPC spectra,[7,8,15–20] and the scaling methodology is still missing.[10]

We propose a methodology to scale the photocurrent spectral density. We also show a simple extension of the photocurrent scaling to determine the sample's responsivity. We derive the methods from the interference of two planar waves. The interference pattern consists of the constant background and the interference term. The absolute value of the constant background relates to the total photocurrent, provided the amplification ratio of the preamplifier is known. The maximal amplitude of the interference term determines the same integral photocurrent. Despite the second method requiring an ideal 50:50 beam splitter, we show that it provides a reliable measurement of the total photocurrent.

We demonstrate the scaling procedures on a calibrated photodiode and SiC interdigital detector. We start with the calibrated InGaAs photodiode (Thorlabs, FGA21-CAL), where the manufacturer provides a National Institute of Standards and Technology (NIST) traceable responsivity spectrum for each diode. The responsivity of the InGaAs diode approaches 1 A/W, allowing the oscilloscope to measure the photovoltage directly. The measure-

ment with an optical bandpass filter provides an accurate optical power measurement. We also show the scaling procedure on a 6H–SiC (II–VI, Inc., semi-insulating, vanadium-doped) interdigital detector. Here, the photoresponse is three orders of magnitude weaker. Therefore, the oscilloscope's sensitivity is insufficient to scale the spectrum with a bandpass filter. We fabricated the interdigital detector using two-step electron beam lithography (Raith 150 Two). The interdigital geometry was defined using dry etching of Ti(5 nm)/Au(15 nm). We used Ti(5 nm)/Cu(85 nm)/Au(15 nm) metalization for wire-bonding. The detector area is 300×300 μm^2.

II. METHODS AND RESULTS

The black curve in Fig. 1(a) shows the Fourier transform Photocurrent Spectrum (FTPS) of the InGaAs diode. The diode is unbiased (photovoltaic detection), and the photocurrent is preamplified by the trans-impedance amplifier (Newport 70710) at the amplification $A_{trans} = 10^4$ V/A (bandwidth 8 MHz). We used a CaF_2 beam splitter and a tungsten white-light source with an aperture of 1 mm to avoid diode saturation. The output photovoltage is carried back in a FTIR spectrometer Bruker Vertex 80v to perform the Fourier transform. The scanner velocity used throughout our experiments was $f_s = 1650$ Hz. Hence, we are well within the bandwidth of the trans-impedance amplifier at 10^4 V/A for all measured wavelengths. The He–Ne laser ($\lambda_{He-Ne} = 633$ nm) measured the mirror position, leading to the wavelength λ harmonic intensity modulation at the frequency f_{mod},

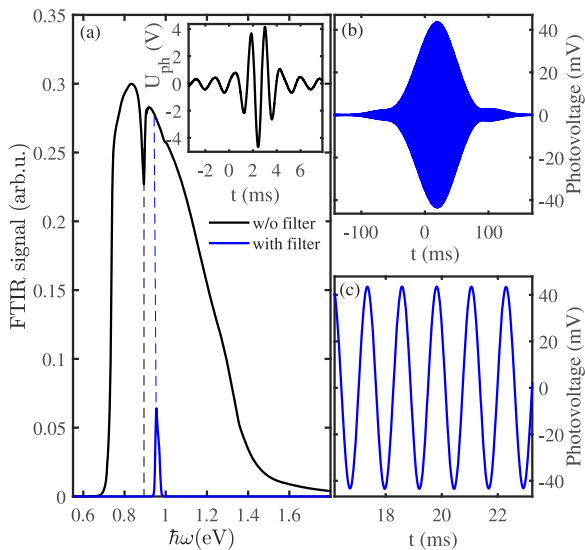$$ f_{mod} = f_s \frac{\lambda_{He-Ne}}{\lambda}. \quad (1) $$

FIG. 1. (a) InGaAs FTPC spectrum measured using the broadband white-light tungsten source (black curve) without and (blue curve) with a bandpass filter (1300 ± 12) nm. The inset shows the interferogram without the bandpass filter measured by the oscilloscope. (b) Full interferogram of the InGaAs diode with the bandpass filter. (c) The interferogram detail is near its maximum as measured by the oscilloscope.

The scaling methods use the relation describing interference of two beams of the intensity I_1 and I_2, resulting in the interference pattern I_m measured with (m = bp) or without (m = tot) the bandpass filter,

$$ I_m = I_{1,m} + I_{2,m} + 2\sqrt{I_{1,m}I_{2,m}} \cos(2k\Delta z)e^{-t/\tau_{coh}}. \quad (2) $$

The wavevector $k = 2\pi/\lambda$ describes the spatial modulation of the monochromatic light at the wavelength λ. The shift in position Δz of the mirror in the Michelson interferometer leads to intensity I_m modulation. The coherence time τ_{coh} describes the reduced visibility of the interference with increasing delay time t. Equation (2) provides two methods to calibrate the spectra. We measure the constant term $I_1 + I_2$ by chopping the light exiting the FTIR spectrometer (the photovoltage is AC-coupled to the preamplifier). We measure this amplified signal by the oscilloscope or by lock-in homodyne detection. The signal $I_1 + I_2$ forms the background of the interferogram; hence, we label these methods by 'back,' or we measure the prefactor $2\sqrt{I_1 I_2}$, assuming $I_1 = I_2$. The total photocurrent is then related to the maximum of the interferogram; hence, we label these methods by "max." Both methods can be measured with or without the bandpass filter. The methods with a bandpass filter are used to calibrate a narrowband spectrum first, and then, the whole spectrum without the bandpass filter is scaled. We call these methods Bandpass Signal Scaling (BSS). The methods without bandpass filter scale directly the full spectrum; hence, we call them Integral Signal Scaling (ISS). Later, we show the equivalence of the four methods and discuss possible scaling errors.

III. BANDPASS SIGNAL SCALING (BSS)

A. BSS-max

The Bandpass Signal Scaling technique relies on the measured FTPC spectrum using a bandpass filter, u^{bp}, the blue curve in Fig. 1(a), and on the measured FTPC spectrum without the bandpass filter, u^{tot}, the black curve in Fig. 1(a). The narrow-band interferogram is measured by the oscilloscope, Fig. 1(b), to determine the maximal photovoltage $U_{BSS,max}$. The photocurrent $I_{BSS,max}$ excited by the narrow-band excitation is related to the measured photovoltage through the trans-impedance amplification A_{trans}, $I_{BSS,max} = U_{BSS,max}/A_{trans}$. Since the measured integrated FTPC signal $F_{tot} = \sum_i u_i^{tot}$ (arb.u.) is proportional to the total photocurrent $I_{BSS,tot}$ (A) and the same proportionality holds for the integrated bandpass FTPC signal $F_{bp} = \sum_i u_i^{bp}$ and $I_{BSS,max}$, the total photocurrent can be scaled as

$$ I_{BSS,tot} = I_{BSS,max} \frac{\sum_i u_i^{tot}}{\sum_i u_i^{bp}} = I_{BSS,max} \frac{F_{tot}}{F_{bp}}, \quad (3) $$

where the summation index i labels points in the measured FTPC spectrum u^{bp} and u^{tot}. The spectra u^{bp} and u^{tot} have to be measured with the same spectral resolution, number of points, and equidistant spacing on the energy axis. Otherwise, the integration elements must be added to the sums in Eq. (3). The spectral current density $\mathscr{I}_{BSS}$ is then determined by

$$ \mathscr{I}_{BSS} = I_{BSS,tot} \frac{u_i^{tot}}{\sum_i u_i^{tot} dE_i} = I_{BSS,tot} \frac{u_i^{tot}}{dE \sum_i u_i^{tot}}, \quad (4) $$

where dE_i is the energy spacing between experimental points u_i^{tot}. The Fourier Transform spectroscopy results in spectra with experimental points equidistant in energy (wavenumber); therefore, the index i can be omitted in dE_i, $dE_i = dE =$ const.

The FTPC spectrum of the InGaAs diode measured with the bandpass filter, the blue curve in Fig. 1(a), has an integral signal $F_{bp} = 55.9$ arb.u. Figures 1(b) and 1(c) show the corresponding interferogram measured by the oscilloscope for two timescales. A detail in Fig. 1(c) shows the interferogram maximum. It resembles the ideal interferogram for monochromatic light. The beating pattern on the timescale ≈ 100 ms, Fig. 1(b), is a fingerprint of the non-ideal monochromatic light. The envelope amplitude of the interferogram should not decay for coherent monochromatic light. The finite coherency leads to the amplitude decay for long delays of the two interfering beams in the Michelson interferometer. Because of the limited coherence time, the correct photovoltage is at zero delay time of the interfering beams. The photovoltage at the maximum of the interferogram is $U_{BSS,max} = 43.55(5)$ mV. Figure 2 shows the scaled photocurrent spectral density using the BSS-max method.

B. BSS-back

The BSS-back method relies on measuring the background intensity $I_1 + I_2$. The background intensity can be measured by chopping the light exiting the FTIR spectrometer and measuring the amplified photovoltage $U_{BSS,back}$ directly by the oscilloscope or by homodyne (lock-in) detection. The photocurrent is then given by $I_{BSS, back} = U_{BSS,back}/A_{trans}$, and formula (3) for the total photocurrent $I_{BSS,tot}$ remains valid when we replace $I_{BSS,max}$ by $I_{BSS,back}$. Formula (4) holds, too.

However, the BSS-back method has two drawbacks. The first one is related to the time response of the measured sample. Suppose there is a frequency-dependent sample's response time. In that case, the homodyne detection has to be performed at the same frequency
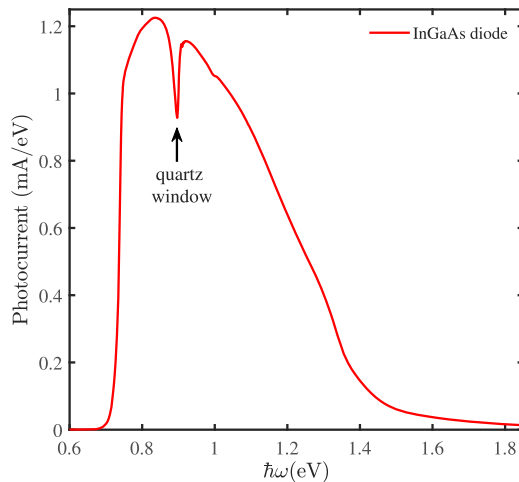
f_{lockin} as the intensity modulation f_{mod} of the light at the bandpass filter selected wavelength λ, Eq. (1), $f_{lockin} = f_{mod}$.

The second drawback is related to the alignment of the Michelson interferometer. If the interferometer is misaligned, the interference term in Eq. (2) becomes reduced, and it might get nullified; however, the background term $I_1 + I_2$ stays unchanged with slight misalignment. We propose this drawback can be used to check the correct alignment of the Michelson interferometer. The alignment verification procedure is as follows:

- Measure the photovoltage with the bandpass filter, $U_{BSS,max}$ (method BSS-max). This photovoltage is measured by intensity modulation at frequency f_{mod}, Eq. (1).
- Measure the photovoltage with the bandpass filter, $U_{BSS,back}$ (method BSS-back). Use the intensity modulation at frequency $f_{lockin} = f_{mod}$. This eliminates the time-response error.
- If $U_{BSS,max} = U_{BSS,back}$, the interferometer is well-aligned at the bandpass wavelength λ.

Applying the BSS-back method to our calibrated InGaAs diode, we get for the background photovoltage, $U_{BSS,back} = 47(2)$ mV.

IV. INTEGRAL SIGNAL SCALING (ISS)

The following two ISS methods are simplifications of BSS methods. The simplification involves measuring the total photocurrent $I_{ISS,tot}$ directly. The ISS methods do not involve a bandpass filter. The photocurrent $I_{ISS,tot}$ is given by the integral of the spectral current density $\mathscr{I}_{ISS}$,

$$I_{ISS,tot} = \int_{E_{min}}^{E_{max}} \mathscr{I}_{ISS}(E)dE. \tag{5}$$

The $I_{ISS,tot}$ has the same meaning as $I_{BSS,tot}$ in Eq. (4). This equivalence is easily shown by inserting Eq. (4) into Eq. (5) and using a Riemann sum as an approximation of the definite integral,

$$I_{ISS,tot} = \int_{E_{min}}^{E_{max}} \mathscr{I}_{ISS}(E)dE = \int_{E_{min}}^{E_{max}} I_{BSS,tot} \frac{u^{tot}(E)}{\sum_i u_i^{tot} dE_i} dE$$

$$\approx \sum_i I_{BSS,tot} \frac{u_i^{tot}}{\sum_i u_i^{tot} dE_i} dE_i = I_{BSS,tot}. \tag{6}$$

Provided $I_{ISS,tot}$ is known, the spectral current density can be calculated using Eq. (4), replacing $I_{BSS,tot}$ by $I_{ISS,tot}$.

A. ISS-max

The method ISS-max involves measuring the prefactor $2\sqrt{I_1 I_2}$, assuming $I_1 = I_2$. The assumption $I_1 = I_2$ is fulfilled in the entire spectral range because both beams experience one reflection and one transmission through the beam splitter. We removed the constant background $I_1 + I_2$ by AC coupling at the input into the oscilloscope. We also assume that zero delays (for all λ) occur at the same mirror position z. If this assumption is fulfilled, then, the maximum of the interferogram corresponds to the spectrally integrated photocurrent $I_{ISS,tot}$.

FIG. 2. InGaAs FTPC spectrum measured using a broadband white-light tungsten source scaled to mA/eV. We scaled the photocurrent by the photovoltage obtained using the bandpass filter (1300 ± 12) nm, method BSS-max.

The inset in Fig. 1(a) shows the interferogram of the pream-plified photocurrent using the InGaAs diode without the bandpass filter. The maximal photovoltage reads $U_{\text{ISS,max}} = 4668(5)$ mV.

B. ISS-back

The ISS-back method relies on determining the prefactor $I_1 + I_2$ of the full-spectrum interferogram. The constant term $I_1 + I_2$ (does not depend on the mirror position z) can be measured by DC coupling or, the excitation light exiting the Michelson inter-ferometer can be chopped; then, homodyne (lock-in, modulation frequency f_{lockin}) detection can be used. The chopped signal can also be measured by the oscilloscope, where the total photocurrent $I_{\text{ISS,back}}$ corresponds to the peak-to-peak value of the rectangular-shaped photovoltage $U_{\text{ISS,back}}$ time dependence. The significant drawbacks of this method are the following. First, in the case of a misaligned interferometer, the interference term $2\sqrt{I_1 I_2}$ might be entirely nullified, and the constant term $I_1 + I_2$ might remain unchanged. Thus, alignment plays a critical role here. The proper alignment can be verified by comparing the results of methods BSS-max and BSS-back, as shown in the alignment verification procedure in Sec. III B.

The second drawback is related to the time response of the sam-ple. Suppose the sample's response time is frequency dependent. In that case, the photocurrent excited by continuous excitation might differ from the photocurrent excited by the intensity-modulated light at the frequency f_{ac}. Thus, the constant term $I_1 + I_2$ measured as a DC photovoltage (behind the trans-impedance amplifier) might differ from the photovoltage measured by the oscilloscope using chopped excitation light at f_{ac} or as measured by the homodyne (lock-in) detection. Since we deal with the spectral integrated signal, here, the complication arises from possible spectral (λ) dependent time response, too. If this is the case, the ISS-back method becomes hardly feasible. We note that the sparse literature on the subject of the FTPC scaling[13] belongs to this class of the ISS-back method. We also note that although the homodyne detection uses the intensity-modulated photo-excitation, the modulation frequency is constant for all measured wavelengths. However, the FTPC spectrum relies on interferogram-modulated photo-excitation, where the intensity modulation is wavelength-dependent, Eq. (1).

The integral photovoltage measured for the calibrated InGaAs diode using the ISS-back method is $U_{\text{ISS,back}}^{(1)} = 5780(50)$ mV.

V. CONSISTENCY OF BSS AND ISS METHODS

The above-described methods lead to consistent photocurrent spectral density scaling, provided the corresponding assumptions on each method are met. In such case, the ratio of the integrated FTPC signal $F_{\text{tot}} = \sum_i u_i^{\text{tot}}$ (arb.u.) to the integrated FTPC signal $F_{\text{bp}} = \sum_i u_i^{\text{bp}}$ measured using the bandpass filter equals the ratio of the photovoltage $U_{\text{ISS,max}}$ and $U_{\text{BSS,max}}$, measured by the ISS-max and BSS-max methods, respectively. This ratio also equals the $U_{\text{ISS,back}}$ and $U_{\text{BSS,back}}$ ratio, measured by the ISS-back and BSS-back methods, respectively. Thus,

$$\frac{F_{\text{tot}}}{F_{\text{bp}}} = \frac{U_{\text{ISS,max}}}{U_{\text{BSS,max}}} = \frac{U_{\text{ISS,back}}}{U_{\text{BSS,back}}}; \quad (7)$$

in addition, when the interferometer is properly aligned,

$$U_{\text{BSS,max}} = U_{\text{BSS,back}}, \quad (8)$$

and in the case of a spectrally independent sample's response time,

$$U_{\text{ISS,max}} = U_{\text{ISS,back}}. \quad (9)$$

The method requiring the least number of assumptions is the BSS-max method, which is the preferable method for scaling. How-ever, for small photo-response samples, it might be difficult to measure the interferogram with the oscilloscope. Hence, the BSS-max procedure might be inapplicable, as we show in Sec. VII for the case of the SiC sample. The advantages and disadvantages of all methods are summarized in Table I.

We compare the results of all scaling methods in Table II. The interferogram maximum measured with the bandpass filter (BSS-max method) is underestimated by 7% compared to the pho-tocurrent determined from the background photo-signal (BSS-back method). The $U_{\text{BSS,back}}$ was measured using a homodyne detection at the frequency $f_{\text{lockin}} = 800(2)$ Hz; the same frequency as the intensity modulation of the bandpass wavelength (1300 nm) at the scanner

TABLE I. Major sources of the scaling error related to the interferometer alignment and the sample's time response.

	Method	Scaling data	Interferometer alignment	Sample's time response
Bandpass signal scaling (BSS)	BSS-max	U_{max}	No scaling error	No scaling error[a]
	BSS-back	U_{back}	Possibly error[b]	Possibly error[c]
Integral signal scaling (ISS)	ISS-max	U_{max}	No scaling error	No scaling error[a]
	ISS-back	U_{back}	Possibly error[b]	Possibly error[d]

[a]The photocurrent spectral components are measured at different modulation frequencies.
[b]If the interferometer is misaligned, the background signal is $I_1 + I_2$, regardless of the misalignment; however, the interference term $2\sqrt{I_1 I_2}$ might be significantly reduced.
[c]No scaling error if $f_{\text{lockin}} = f_{\text{mod}}$. The homodyne frequency of the intensity modulation f_{lockin} should match the frequency f_{mod} of the bandpass (bp) filter selected wavelength λ_{bp}, related to the scanner velocity v_s of the Michelson interferometer, $f_{\text{mod}} = 2v_s/\lambda_{\text{bp}}$.
[d]If the sample's response is frequency dependent in the frequency range $(2v_s/\lambda_{\text{max}}, 2v_s/\lambda_{\text{min}})$.

TABLE II. Comparison of the integrated FTIR signal and photovoltage measured with and without a bandpass filter for the InGaAs calibrated photodiode and the SiC interdigital detector.

Sample	Total signal (ISS)	Signal with bandpass filter (BSS)	Ratio
InGaAs–FTPC signal	F_{tot} = 6313 arb.u.	F_{bp} = 55.9 arb.u.	113.0
Interferogram U_{max}	$U_{ISS,max}$ = 4668(5) mV	$U_{BSS,max}$ = 43.55(5) mV	107(3)
Interferogram U_{back}–pk-pk	$U_{ISS,back}$ = 5780(50) mV	$U_{BSS,back}$ = 47(2) mV	123(5)
SiC–FTPC signal	F_{tot} = 48.7 arb.u.	F_{bp} = 0.57 arb.u.	85.3
Interferogram U_{max}	$U_{ISS,max}$ = 31.1 mV	NA	NA
Interferogram U_{back}–pk-pk	$U_{ISS,back}$ = 66.2(5) mV	NA	NA
Interferogram U_{back}–rms	$U_{ISS,back}$ = 24.8(5) mV	$U_{BSS,back}$ = 0.29(5) mV	85(15)

velocity 1650 Hz, Eq. (1), f_{mod} = 803 Hz. Thus, the sample's response time does not cause the 7% underestimation if we neglect the higher harmonic response of the InGaAs diode to the rectangular-like photo-excitation. We used the optical chopper to modulate the light exiting the interferometer; however, the interferometric modulation is harmonic in time.

The underestimation of the total photocurrent measured by the maximum of the interferogram (ISS-max method) is increased to 19% compared to the background measured total photocurrent (ISS-back method). This increased underestimation demonstrates a slight misalignment of the Michelson interferometer. The misalignment is more prone to errors for shorter wavelengths. Since the error 7% occurs in the long-wavelength part of the spectrum (1300 nm), the alignment error is enhanced for shorter wavelengths (<1300 nm), and the underestimation of the total photocurrent increases to the measured 19%. Part of the 19% error could also be caused by the frequency-dependent response time of the InGaAs diode.

The ratios F_{tot}/F_{bp}, $U_{ISS,max}/U_{BSS,max}$, and $U_{ISS,back}/U_{BSS,back}$, Table III, satisfy the consistency condition Eq. (7) within 16% precision. Figure 2 depicts the BSS-max scaled photocurrent spectral density of the InGaAs diode. The quartz window caused the dip at 0.89–0.90 eV at the output of the FTIR spectrometer. The quartz window allows evacuation of the FTIR spectrometer Bruker Ver-

TABLE III. Quantities used to calculate the InGaAs diode's responsivity and photocurrent in FTPC spectra.

Quantity	Value	Rel. accuracy (%)
Amplification[a]	$(10^4 \pm 10^2)$ V/A	1
Intensity[b]	(6.27 ± 0.31) μW	5
Photovoltage[c]	(47 ± 2) mV	4.3
Responsivity	(0.75 ± 0.05) A/W	6.7
Data-sheet responsivity[d]	(0.733 ± 0.040) A/W	5

[a]Trans-impedance preamplifier Newport 70710.
[b]Tungsten white-light source, measured by the Thorlabs sensor S122C 700–1800 nm, 40 mW behind the Thorlabs bandpass filter FB1300-12.
[c]Measured using the Thorlabs, InGaAs FGA21-CAL, photovoltaic configuration, plugged in the Bruker Vertex 80v FTIR spectrometer.
[d]Thorlabs, InGaAs FGA21-CAL.

tex 80v and simple manipulation with the excitation light beam (focusing) and sample (positioning) located outside the evacuated space.

VI. RESPONSIVITY SCALING

We resolved the spectrally unequal white-light intensity effects by normalizing the photocurrent spectrum by the white-light power spectrum $P_{exc,j}$. Besides the photocurrent scaling, the responsivity scaling also requires the absolute measurement of the optical power P, $R = I/P$. A typical optical power gauge is calibrated for a given wavelength λ. Hence, the responsivity scaling has to be performed using a bandpass filter, and only BSS methods apply here ($I = I_{BSS,max}$ or $I = I_{BSS,back}$). We scale the responsivity R_j (index j labels points in the FTPC spectrum) in the whole measured spectral range by using the bandpass FTPC spectrum u^{bp} as a weighting function w_i, normalized such as $\sum_i w_i = 1$; the index i labels the experimental data on a discrete energy scale, $w_i = \frac{u_i^{bp}}{\sum_i u_i^{bp}}$. The scaled FTPC responsivity spectrum R_j is then

$$R_j = \frac{u_j^{pwr}}{\sum_i w_i u_i^{pwr}} R_{bp},\qquad(10)$$

where $u_i^{pwr} = u_i^{tot}/P_{exc,i}$ is the spectral power $P_{exc,i}$ normalized FTPC signal u_i^{tot}. We measured the white-light power P_{bp} behind the bandpass filter and determined the responsivity $R_{bp} = I_{tot,bp}/P_{bp}$ at 1300 nm. We calibrated the responsivity using a bandpass filter (FB1300-12, Thorlabs) transmitting only wavelengths in the band (1300 ± 12) nm. The blue peak in Fig. 1(a) depicts the bandpass FTIR spectrum of the InGaAs diode.

We summarize the results of the calibrated InGaAs diode responsivity scaling in Table III. The responsivity is within a 5% error in agreement with the specification provided by the manufacturer (Thorlabs).

We show the responsivity of the InGaAs diode in Fig. 3. The agreement with the specification is within the entire spectral range at the level of 5%. We note that it is essential to use a calibrated photodiode. The photodiodes differ from piece to piece, and their responsivity can be distinct from the typical diode characteristics, as shown in Fig. 3. The primary source of error is the absolute measurement of the optical power and measurement of the white-light spectrum.
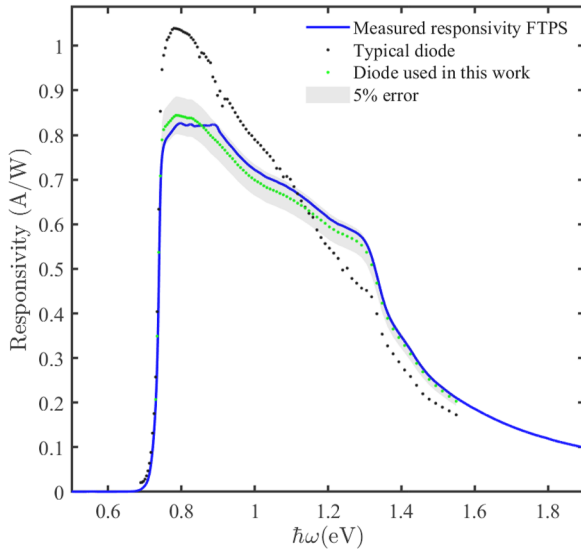
FIG. 3. Responsivity of InGaAs diode provided by Thorlabs for (black points) typical diode and (green points) our particular diode FGA21-CAL including 5% error margin. (solid blue curve) The measured and scaled responsivity spectrum.

FIG. 4. (a) As-measured FTPC spectrum of the SiC interdigital detector (black curve) without and (blue curve) with a bandpass filter. The inset shows the interferogram of the full spectrum without a bandpass filter. These data are the oscilloscope-measured interferogram behind the trans-impedance preamplifier. (b) Data scaled to (left scale, blue curve) responsivity and (right scale, red curve) photocurrent spectral density.

VII. SMALL PHOTOCURRENT AND FREQUENCY-DEPENDENT RESPONSE TIME

The advantage of the InGaAs diode is its high responsivity. In this section, we demonstrate the scaling procedure of the weakly responsive SiC interdigital detector and show the effects of the frequency-dependent response time. Figure 4(a) depicts the FTPC spectrum of the SiC interdigital detector measured without the bandpass filter (black curve) and with the 1300 nm bandpass filter (blue curve) using a trans-impedance amplification $A_{\text{trans}} = 10^8$ V/A. The inset in Fig. 4(a) shows the interferogram of the FTPC spectrum measured without the bandpass filter, and the arrow points to the maximum of the interferogram showing the total photovoltage $U_{\text{ISS,max}} = 31.1$ mV (method ISS-max). The interferogram signal is very weak when the photovoltage is measured with the bandpass filter. Therefore, we could not use the BSS-max method ($U_{\text{BSS,max}} = $ NA). However, $U_{\text{BSS,max}} = U_{\text{BSS,back}}$ holds in the case of a well-aligned interferometer. We verified good alignment of the interferometer in the case of the InGaAs diode. We measured $U_{\text{BSS,back}} = 0.29(5)$ mV by a homodyne detection at $f_{\text{lockin}} = 800$ Hz. The photovoltage $U_{\text{BSS,back}}$ is clearly below the sensitivity of a common oscilloscope, requiring homodyne detection.

The photovoltage measured without the bandpass filter shows a large variation depending on the experimental technique. In all cases, we chop the light exiting the Michelson interferometer at $f_{\text{lockin}} = 800$ Hz. The ISS method results in $U_{\text{ISS,back}}^{\text{pk-pk}} = 66.2(5)$ mV from the peak-to-peak value measured by the oscilloscope, and it results in $U_{\text{ISS,back}}^{\text{rms}} = 24.8(5)$ mV measured by the homodyne detection. The homodyne detection provides the root-mean-square (rms) value of the photovoltage time dependence. The peak-to-peak photovoltage $U_{\text{pk-pk}}$ is related to the rms value $U_{\text{rms}} = 0.5U_{\text{pk-pk}}$
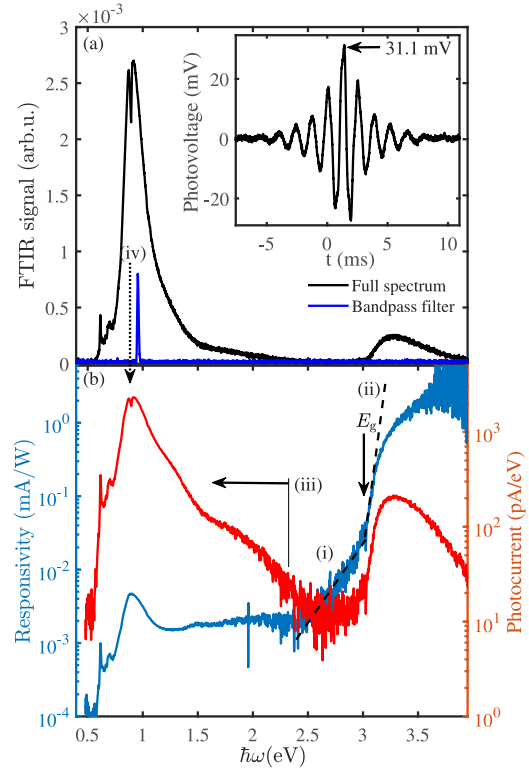
for the square-wave, or $U_{\text{rms}} = \frac{U_{\text{pk-pk}}}{2\sqrt{2}} = 0.35U_{\text{pk-pk}}$ for a harmonic waveform. We experimentally determined $U_{\text{ISS,back}}^{\text{pk-pk}}/U_{\text{ISS,back}}^{\text{rms}} = 0.37$, which is closer to the harmonic waveform, signifying the sample's long response time ($\tau > 1/f_{\text{lockin}} \approx 1$ ms). Despite the long response time, the ratio $\frac{F_{\text{tot}}}{F_{\text{bp}}} = 85.3$ equals within an experimental uncertainty $\frac{U_{\text{ISS,back}}}{U_{\text{BSS,back}}} = 85(15)$, Eq. (7). This agreement leads us to conclude that the response time is negligible in the FTPC scaling of the SiC interdigital detector. The red FTPC spectrum shows the scaled photocurrent spectral density of the 6H–SiC detector in Fig. 4(b).

The measured optical power behind the bandpass filter $P_{\text{bp}} = 6.3(3)$ µW allows calculating the responsivity spectrum, Eq. (10). The blue spectrum in Fig. 4(b) shows the responsivity of the 6H–SiC interdigital detector.

In the following paragraph, we study the effect of the sample's long response time. We compare two experimental methods to measure responsivity in Fig. 5. The black curve shows the FTPC responsivity, and the red points result from the monochromator-based measurement using a homodyne detection at $f_{\text{lockin}} = 200$ Hz. The responsivities match below 1 eV and near the bandgap of SiC. The low efficiency of the prism in the UV spectral range causes erroneous responsivity in the monochromator-based measurement
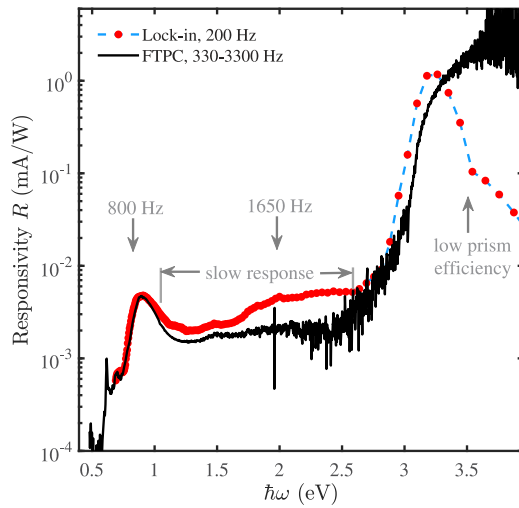
FIG. 5. (black curve) FTPC responsivity is compared to the (red points–blue dashed curve) responsivity measured by the monochromator and phase-sensitive homodyne detection (lock-in). The frequencies 800 and 1650 Hz of the FTPC modulation are shown for two selected wavelengths by gray text arrows.

above the SiC bandgap. The slow sample response causes the lower FTPC responsivity in the 1.2–2.7 eV range. In this range, the photocurrent is modulated at 200 Hz when measuring the photocurrent using a monochromator and homodyne detection. However, the photocurrent is modulated at frequencies 1.0–2.3 kHz, Eq. (1), using FTPC spectroscopy. The spectral range 1.2–2.7 eV corresponds to the slow mid-gap to conduction band transitions. The FTPC modulation frequencies are very high for these slow transitions to match the responsivity of the slower (200 Hz) light modulation used with the monochromator-based homodyne detection of the photocurrent.

VIII. DISCUSSION

The responsivity of the SiC interdigital detector shows the onset of the optical absorption for photon energies $\hbar\omega$ larger than bandgap E_g = 3.06 eV. This absorption onset reflects the expected bandgap of the 6H–SiC polytype. These interband transitions are one to two orders of magnitude stronger than the impurity-band transitions in the responsivity spectrum. The indirect bandgap of SiC appears as two distinct slopes of the absorption edge, shown by dashed lines (i) and (ii) in Fig. 4(b). The low-energy/high-energy part (i)/(ii) corresponds to the photon absorption assisted by the phonon's simultaneous absorption/emission. The transitions from the deep-level states to the conduction band dominate the absorption for energies $\hbar\omega < E_g$. The Fermi level $E_F \approx E_c - 0.8$ eV. The photoconductivity peak near 1 eV is related to the states pinning the Fermi level, thus compensating for the background doping in the semi-insulating SiC.

We point out that FTPC spectroscopy is a sensitive technique providing valuable information about deep levels in semiconductors and interband transitions. The photocurrent sensitivity of the order of 100's fA is related to the Fourier transform narrowed noise

bandwidth Δf_{noise}. FTPC spectroscopy probes the full photoconductivity spectrum $(\lambda_{\min}, \lambda_{\max})$ at once by intensity modulation of the wavelength λ at the frequency f_{mod}, Eq. (1). Therefore, the FTPC is a broadband technique. The noise added to the signal limits the smallest detectable signals, as described by the signal-to-noise ratio. The noise strength is related to the noise frequency bandwidth contributing to the measured signal. The noise bandwidth in the FTPC spectroscopy is related to the spectral resolution $\Delta\nu$ of the measured FTPC spectrum. Differentiating Eq. (1) with respect to the wavenumber $\nu = 1/\lambda$, we get for the noise bandwidth

$$\Delta f_{\text{noise}} = f_s \lambda_{\text{He-Ne}} \Delta\nu. \tag{11}$$

The set spectral resolution ($\Delta\nu$ = 8 cm^{-1}) and the scanner velocity f_s = 1650 Hz give the noise bandwidth Δf_{noise} = 0.8 Hz after performing the Fourier transform. Such a narrow bandwidth significantly enhances the signal-to-noise ratio, allowing to measure small photocurrent signals.

The primary issue of the scaling method described here is the case of small signals and samples with long response times. When the oscilloscope cannot measure the interferogram of small signals using a beam splitter directly, the integral scaling methods (ISS-max or ISS-back) must be used. The first assumption on the valid scaling is that the beam splitter in the Michelson interferometer splits the beam precisely in the ratio of 50:50. Second, the interfering wavelengths show zero delays at the same mirror position. The non-zero delay between the two beams might appear when the dispersion of the index of refraction of the beam splitter is very large. The construction of the beam splitter in the FTIR spectrometer Vertex 80v compensates the dispersion by assuring that both interfering beams travel the same distance through the beam splitter and experience the same number of transmissions and reflections under the same angles. However, the non-ideal construction can lead to slightly different optical paths. This non-ideality leads to spatially shifted interferogram maxima for different wavelengths. In such a situation, the maximal photovoltage would be a meaningless quantity. The frequency and spectrally dependent sample response might also be an issue. However, as we demonstrated in the case of slow SiC samples, this error can be mitigated by the BSS method using a homodyne measurement scheme of the photocurrent.

IX. CONCLUSIONS

We described a methodology to scale the FTPC spectra to photocurrent spectral density (A/eV). We also presented a method for responsivity (A/W) scaling. We formulated conditions that have to be met to avoid erroneous scaling caused by the interferometer misalignment or sample response time. We verified the method on a NIST traceable calibrated InGaAs photodiode and applied the technique to the slow 6H–SiC interdigital detector.

ACKNOWLEDGMENTS

AUTHOR DECLARATIONS

Conflict of Interest

The authors have no conflicts to disclose.

Author Contributions

J.K.: Conceptualization, sample fabrication, lithography, data analysis, methodology, writing the original draft and editing, funding, B.M.: measurements, data analysis, draft editing, M.S.: Sample preparation, T.F.: Samples' fabrication, lithography, V.D.: experimental support, draft review.

J. Kunc: Conceptualization (lead); Data curation (lead); Formal analysis (lead); Funding acquisition (lead); Investigation (equal); Methodology (lead); Project administration (lead); Resources (lead); Supervision (lead); Validation (lead); Visualization (lead); Writing – original draft (lead); Writing – review & editing (equal). **B. Morzhuk**: Data curation (equal); Investigation (equal); Methodology (equal); Validation (equal); Visualization (supporting); Writing – review & editing (equal). **M. Shestopalov**: Investigation (equal). **T. Fridrišek**: Investigation (equal); Writing – review & editing (supporting). **V. Dědič**: Conceptualization (supporting); Investigation (supporting); Validation (equal); Writing – review & editing (supporting).

DATA AVAILABILITY

The data that support the findings of this study are available from the corresponding author upon reasonable request.

REFERENCES

[1] H. W. H. M. Jongbloets, J. H. M. Stoelinga, M. J. H. van de Steeg, and P. Wyder, Phys. Rev. B **20**, 3328 (1979).

[2] C. Q. Chen, J. Zeman, F. Engelbrecht, C. Peppermüller, R. Helbig, Z. H. Chen, and G. Martinez, J. Appl. Phys. **87**, 3800 (2000).

[3] M. Vanecek and A. Poruba, Appl. Phys. Lett. **80**, 719 (2002).

[4] E. Lavrov, F. Borrnert, and J. Weber, Phys. Rev. B **72**, 085212 (2005).

[5] H. Frenzel, H. von Wenckstern, A. Weber, H. Schmidt, G. Biehne, H. Hochmuth, M. Lorenz, and M. Grundmann, Phys. Rev. B **76**, 035214 (2007).

[6] H. Pettersson, L. Landin, Y. Fu, M. Kleverman, M. Borgström, W. Seifert, and L. Samuelson, in *5th International Conference on Low Dimensional Structures and Devices (LDSD 2004), Cancun, Mexico, 2004* [Microelectron. J. **36**, 227 (2005)].

[7] L. Höglund, C. Asplund, Q. Wang, S. Almqvist, H. Malm, E. Petrini, J. Y. Andersson, P. O. Holtz, and H. Pettersson, Appl. Phys. Lett. **88**, 213510 (2006).

[8] R. Kravets, K. Johnston, J. Potmesil, V. Vorlicek, and M. Vanecek, in *16th European Conference on Diamond, Diamond-Like Materials, Carbon Nanotubes, and Nitrides, Toulouse, France, 2005* [Diamond Relat. Mater. **15**, 559 (2006)].

[9] J. Holovský, S. De Wolf, J. Werner, Z. Remeš, M. Müller, N. Neykova, M. Ledinský, L. Černá, P. Hrzina, P. Löper, B. Niesen, and C. Ballif, J. Phys. Chem. Lett. **8**, 838 (2017).

[10] K. Ridzonova, R. Grill, A. P. Amalathas, B. Dzurnak, N. Neykova, L. Horak, P. Fiala, X. Y. Chin, C. M. Wolff, Q. Jeangros, and J. Holovsky, J. Mater. Chem. A **10**, 18928 (2022).

[11] A. Hikavyy, P. Clauws, W. Deferme, G. Bogdan, K. Haenen, and M. Nesladek, in *10th International Workshop on Surface and Bulk Defects in CVD Diamond Films, Diepenbeek Hasselt, Belgium, 2005* [Phys. Status Solidi A **202**, 2171 (2005)].

[12] J. Holovský, in *Fourier Transforms: New Analytical Approaches and FTIR Strategies*, edited by G. Nikolic (IntechOpen, Rijeka, 2011), Chap. 13.

[13] N. Puspitosari and C. Longeaud, Rev. Sci. Instrum. **88**, 086112 (2017).

[14] K. Vandewal, L. Goris, I. Haeldermans, M. Nesládek, K. Haenen, P. Wagner, and J. V. Manca, in *Symposium on Advanced Materials and Concepts for Photovoltaics held at the EMRS 2007 Conference, Strasbourg, France, 2007* [Thin Solid Films **516**, 7135 (2008)].

[15] A. Kromka, R. Kravetz, A. Poruba, J. Zemek, V. Perina, J. Rosa, and M. Vanecek, in *8th International Workshop on Surface and Bulk Defects in CVD Diamond Films, Diepenbeek Hasselt, Belgium, 2003* [Phys. Status Solidi A **199**, 108 (2003)].

[16] K. Haenen, M. Nesládek, L. De Schepper, R. Kravets, M. Vaněček, and S. Koizumi, in *9th International Conference on New Diamond Science and Technology, Waseda University, Tokyo, Japan, 2004* [Diamond Relat. Mater. **13**, 2041 (2004)].

[17] L. Goris, A. Poruba, L. Hoďakova, M. Vanecek, K. Haenen, M. Nesladek, P. Wagner, D. Vanderzande, L. De Schepper, and J. V. Manca, Appl. Phys. Lett. **88**, 052113 (2006).

[18] J. Holovský, U. Dagkaldiran, Z. Remeš, A. Purkrt, T. Ižák, A. Poruba, and M. Vaněček, Phys. Status Solidi A **207**, 578 (2010).

[19] E. C. I. Enobio, H. Sato, K. Ohtani, Y. Ohno, and H. Ohno, Jpn. J. Appl. Phys. **51**, 06FE15 (2012).

[20] K.-M. Guenther, T. Gimpel, J. W. Tomm, S. Winter, A. Ruibys, S. Kontermann, and W. Schade, Appl. Phys. Lett. **104**, 042107 (2014).

25 January 2024 11:45:21